**Proceedings of 15th IOE Graduate Conference**
*Peer Reviewed*
Year: 2024 Month: May Volume: 15
ISSN: 2350-8914 (Online), 2350-8906 (Print)

# Geogrid Reinforced Flexible Pavement: Thickness Reduction Potential and Increment in Service Life

Kabin Lamichhane [a], Dhanapati Dhakal [b], Bijay Bhattarai [c]

[a,b,c] *Department of Civil Engineering, Institute of Engineering, Thapathali campus, Tribhuvan University*
[a] kabin.762416@thc.tu.edu.np , [b] dhanapati.076bce039@tcioe.edu.np , [c] bijay.076bce029@tcioe.edu.np

**Abstract**
This study performs a numerical analysis to evaluate the effectiveness of single-layer geogrid-reinforced flexible pavement, with the geogrid positioned optimally. The analysis takes into account varying California bearing ratio (CBR) values of subgrade, which range from 5% to 15%, and traffic loads that span from 5 million standard axle (MSA) to 30 million standard axle (MSA). The analysis is carried out with the aid of PLAXIS 3D, a finite element method (FEM) based software. A linear elastic model simulated pavement layers (asphalt course, combined granular base and subbase course and subgrade), and initial validation compared vertical subgrade strain for unreinforced pavement with IITPave's and DoR sheet's results. Results show that the subbase and subgrade interface is the optimum position for geogrid reinforcement. Significant thickness reduction is possible in existing unreinforced flexible pavements after geogrid insertion, with increase in service life as well. Based on the study results, a geogrid-reinforced pavement design catalogue is proposed and compared with the existing Department of Roads, Nepal (DoR) flexible pavement design guidelines, 2021. The study also investigates the lifespan improvement of the reinforced pavement layer compared to the unreinforced one.

**Keywords**
Flexible Pavement, Geogrid Reinforcement, Optimum Position, Thickness Reduction, Performance Enhancement

## 1. Introduction

A multi-layered elastic structure, envisioned as a flexible pavement, is constructed over subgrade soil and a natural foundation to facilitate vehicular movement. The highest load-bearing material is on the top layer, decreasing towards the bottom. A standard flexible pavement Figure 1a includes asphalt concrete (surface and binder courses) on top, followed by granular base and sub-base layers, and a compacted soil subgrade [1, 2, 3]. The stresses generated by the movement of vehicles are transmitted through the granular structure via grain-to-grain contact of aggregates. The primary failure in flexible pavement Figure 1b is fatigue cracking at the asphalt base material interface and rutting at the sub-base subgrade interface [2]. Fatigue cracking, resembling an alligator's back, is linked to tensile strain in the hot mix asphalt layer, while rutting results from cumulative vertical strain in sublayers. Both distress types contribute to critical pavement responses [2, 3, 4, 5, 6].

The growing scarcity of conventional construction materials such as aggregates, driven by environmental concerns and legal restrictions on quarrying, is happening concurrently with a significant expansion in construction activity. In this scenario, it's crucial to use techniques to reduce pavement thickness and enhance durability. Geosynthetics, such as geogrids, geotextiles, geocells, geomembranes, geo-composites, and more, prove beneficial in reducing pavement thickness and enhancing other properties [7, 8]. These include prevention of pavement surface from reflective cracking, subgrade separation, stabilization, base or sub-base reinforcement, and overlay stabilization when strategically integrated within and between the layers of the pavement [9].

Among geosynthetics, geogrid is widely employed in pavement systems for its potential to reduce base course thickness and increasing service life [7, 9, 10, 11].

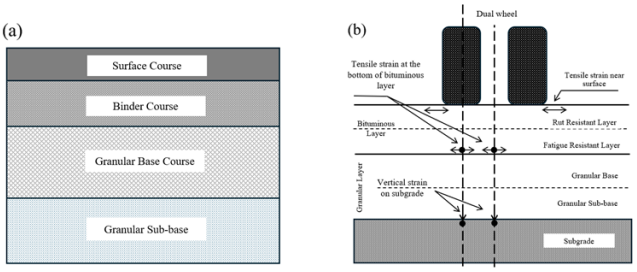


**Figure 1:** Pavement section with: (a) four typical layer (b) critical location of failure (modified from [2])

Geogrid operates on three fundamental mechanisms: (a) Lateral restraint (Figure 2a), (b) improved bearing capacity (Figure 2b), and tensioned membrane effect (Figure 2c). Lateral restraint confines aggregate material during loading, restricting its lateral flow. Enhanced confinement improves base course modulus, enhancing stress distribution on the subgrade and reducing surface strain. Improved bearing capacity shifts the failure envelope from weaker subgrade to stronger base course material. The tensioned membrane effect relies on tensile stress in a deformed membrane, enhancing vertical stress distribution [8, 12]. The optimum efficiency of geogrid in reinforcing pavement systems is attained by placing it in the optimum position.

Literature presents a range of perspectives on the optimum positioning of geogrids. [12] suggested deeper geosynthetic placement in granular course enhances performance for

heavy traffic, while shallower placement benefits roads with lighter traffic. [9, 13] shows that geogrid integration at the sub-base-subgrade interface in flexible pavements enhances performance by extending service life or reducing structural thickness while maintaining equivalent functionality. [14] concluded that the use of geogrid reinforcement resulted in a more evenly distributed load and a reduction in rut depth at the surface of the asphalt course. [1, 14, 15, 16] have discovered, through field evidence and theoretical studies, that the service life of flexible pavements can be prolonged by incorporating geogrids at the asphalt base interface.

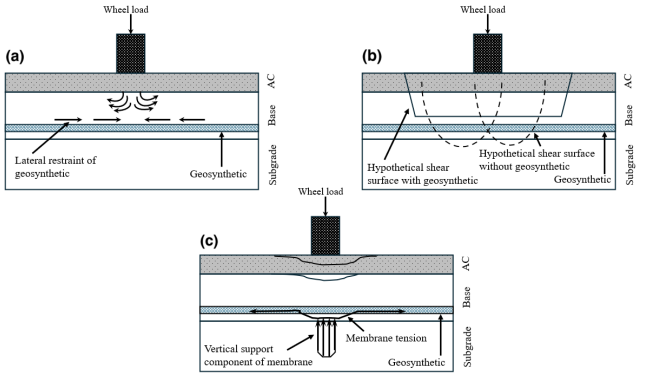


**Figure 2:** Reinforcement mechanism of geogrid by: (a) lateral spread, (b) bearing capacity, and (c) tensioned membrane (modified from [12])

However, most studies assessing the effect of geogrid on flexible pavement focus on low CBR soil and a limited range of traffic loads. For this reason, the study of geogrid reinforced flexible pavement built over relatively with strong CBR can bridge the existing gap. This study aimed to determine the optimum placement of geogrid, potential thickness reduction, and enhancements in durability through numerical modeling. Finite element modeling, particularly linear elastic modeling with Plaxis 3D, was utilized for this purpose. The geogrid is placed from the asphalt-granular base interface down to depths of 20%, 40%, 60%, and 80% of the granular course thickness before reaching the granular base-subgrade interface to asses optimum position. The design of geogrid-reinforced pavements heavily relies on factors like soil layers, geogrid properties, and traffic loads with each design requires specific analysis and calculations [8]. The existing design code lacks of dedicated catalogs for reinforced pavement design. After this study, a new design catalogue for optimum geogrid-reinforced flexible pavement is proposed, with calculations for the potential increase in service life after geogrid integration.

## 2. Methodology

This study conducts numerical analysis for both reinforced and unreinforced pavements using FEM aided Plaxis 3D for various subgrade strengths CBR varying from 5% to 15% and traffic loads from 5 MSA to 30 MSA, modeling flexible pavements as two-layer structure; subbase and base combined is considered as granular course, dense bituminous macadam (DBM) and asphalt layer combined is considered as asphalt course. Vertical compressive strain at the top of subgrade is computed using a linear elastic model. The study demonstrates the advantages of geogrid reinforcement, particularly in terms of reducing pavement thickness and service life ratio [3, 8]. The detail approach for designing geogrid-reinforced flexible pavements is explained here.

Step 1: In the initial phase of designing geogrid-reinforced flexible pavement, the thickness of different pavement layers i.e., subbase, base, DBM, and AC is determined based on the design specifications provided in [2], which are dependent on the CBR value of subgrade and traffic load.

Step 2: The pavement layer is conceptualized as a two-layer system. Resilient modulus calculations for the subgrade, granular course, and asphalt course are conducted using empirical relations outlined in [2] as demonstrated in Table 1.

Step 3: Numerical models formulated in Plaxis 3D are employed to determine vertical compressive strain at the top of subgrade. This process utilizes input parameters such as the modulus of different pavement layers, their respective thicknesses, the saturated and the unsaturated unit weights, and Poisson's ratio, following the guidelines provided by [2].

Step 4: The limiting strain values are derived from the rutting and fatigue models outlined in [2]. Table 2 illustrates rutting and fatigue models as provided in [2]. Strain and deformation values are additionally computed utilizing DOR sheet and IITPave software. Validation work has been conducted to ensure accuracy.

Step 5: Multiple numerical simulations are conducted in Plaxis 3D by adjusting the placement of the geogrid within the thickness of the granular course. The interface between the granular course and the asphalt course, i.e., the top of the granular course, is denoted as "geogrid position 0%". Similarly, the interface between the granular course and the subgrade course, i.e., the bottom of the granular course, is labeled as "geogrid position 100%". Intermediate positions of the geogrid are named based on the distance from the "geogrid position 0%" relative to the total thickness of the granular layer.

Step 6: Vertical compressive strain at the top of subgrade is computed for CBR value 5% to 15% with geogrid positions 0%, 20%, 40%, 60%, 80%, and 100% in each condition. These values are compared, and the smallest value among geogrid position 0% to 100% of each CBR is selected to represent the optimum position of the geogrid.

Step 7: Through repeated hit and trials methods, the height of the granular course in the reinforced pavement is reduced to achieve an equal/near to equal subgrade strain value as observed in the unreinforced pavement model.

Step 8: The service life ratio is determined based on the vertical compressive strain experienced by the

subgrade in both reinforced and unreinforced pavement scenarios. It is calculated using the formula SLR = $\varepsilon$v1/$\varepsilon$v2 Where, $\varepsilon$v1 represents the vertical compressive strain on the subgrade in the unreinforced case, while $\varepsilon$v2 denotes the vertical compressive strain on the subgrade in the reinforced case. These steps are repeated across various combinations of CBR values and traffic loads to recommend a new design catalog specifically tailored for geogrid-reinforced flexible pavement.

**Table 1:** Resident Modulus

| Pavement Layers | Resilient Modulus |
|---|---|
| Asphalt course | $M_B$ = 2000MPa |
| Base/Subbase (Granular course) | $M_{RGRAN}$ = 0.2×(h)$^{0.45}$ ×$M_{RSUPPORT}$ |
| Subgrade (CBR ≤ 5%) | $M_{RS}$ = 10.0× CBR |
| Subgrade (CBR > 5%) | $M_{RS}$ = 17.6×(CBR) $^{0.64}$ |

Where, $M_B$ is the resilient modulus of the asphalt course, $M_{RGRAN}$ is the resilient modulus of the granular course (MPa), h is the thickness of the granular course in mm, $M_{RS}$ is the resilient modulus of the subgrade soil (MPa), CBR is the California bearing ratio of the subgrade soil (%).

**Table 2:** Rutting and Fatigue models

| Proposed model | Empirical relation |
|---|---|
| Rutting model | NR= $4.1656\times10^{-8}\times(1/\varepsilon v)\times4.5337$ (for 80% reliability) |
| | NR = $1.41\times10^{-8}\times(1/\varepsilon v)\times4.5337$ (for 90% reliability) |
| Fatigue model | Nf= $1.6064\times C\times10^{-4}(1/\varepsilon t)\times3.89\times(1/MRm)\times0.854$ (for 80% reliability) |
| | Nf = $0.5161\times C\times10^{-4}\times(1/\varepsilon t)\times3.89\times(1/MRm)\times0.854$ (for 90% reliability) |
| | Where, C = 10M , M = $4.84\times(\frac{V_{be}}{V_a+V_{be}}-0.69)$ |

NR=subgrade rutting life in number of standard axles, $\varepsilon$v=vertical compressive strain at the top of the subgrade, Va =Percent volume of air void in the bitumen mix, Vbe = Percent volume of effective bitumen in the mix. Nf =Fatigue life of bituminous layer in number of standard axles, $\varepsilon$t =Maximum horizontal tensile strain at the bottom of the asphalt course, MRm =Resilient modulus (MPa) of the asphalt course.

## 3. Numerical Model

This section provides a concise overview of the numerical examination of both unreinforced and reinforced flexible pavements, employing FEM software, Plaxis 3D. For result assessment derived from the numerical analysis, DoR sheet and IITPave serves as the reference standard.

### 3.1 Geometry, Material Properties and Loading

Two lane highway with 3.5m carriageway and 0.75m shoulder for each lane resulting in 8.5m is considered as the width of the pavement and length is taken as 10m. Thickness of base, subbase, DBM and AC is taken from [2]. The subgrade soil is infinite below ground in real scenario but for modelling purpose, the thickness of it is taken as 3m by knowing load effect at this depth will be negligible.

**Table 3:** Material properties

| Identification | Drainage type | $\gamma_{sat}$ | $\gamma_{unsat}$ | Poison ratio |
|---|---|---|---|---|
| Subgrade | Undrained | 20 | 18 | 0.35 |
| Granular layer | Drained | 21 | 19 | 0.35 |
| Asphalt layer | Non-porous | - | 20 | 0.35 |
| Geogrid stiffness = 700 kN/m | | | | |
| where $\gamma_{sat}$ = Saturated unit weight, $\gamma_{unsat}$ = Unsaturated unit weight | | | | |

### 3.2 Boundary conditions and Mesh discretization

In the process of calculating stresses and strains within a model, each Finite Element Method software conducts an iterative analysis aimed at converging to a solution that meets specified boundary conditions. The choice of boundary conditions is crucial, requiring that displacements or strains near the boundaries in all three directions accurately reflect the real conditions at the site [17]. Plaxis 3D uses automatic process to give such conditions which are shown in Table 4.

**Table 4:** Mesh options and Boundary conditions

| Mesh options | Assigned Value | Boundary | Boundary condition |
|---|---|---|---|
| Relative element size | 0.5 | $X_{min}$ | Normally fixed |
| Element dimension | 0.5 | $X_{max}$ | Normally fixed |
| Use enhanced refinements | True | $Y_{min}$ | Normally fixed |
| Global scale factor | 0.2 | $Y_{max}$ | Normally fixed |
| Minimum element size factor | 0.01 | $Z_{min}$ | Fully fixed |
| Swept meshing | True | $Z_{max}$ | Free |

Creating a suitable finite element mesh is a crucial step that connects the definition of geometry with the construction phases. Numerical stability throughout the calculation requires a high-quality mesh, where elements are regular and not overly elongated or thin. PLAXIS 3D utilizes a fully automatic process to generate finite element meshes, considering factors such as soil layers, structural components, loads, and boundary conditions [17]. The soil's condition at the soil-structure interface is crucial in determining the reduction factor for interface elements. For seamless interaction among different pavement layers, a reduction factor '$R_{int}$' of 1 is assumed. The pavement response model assumes complete contact between the geogrid and the pavement layer [18]. The meshing parameters used in this

study are given in Table 4. The nodes in element and discretized mesh for the geometry used in this study is shown in Figure 3.

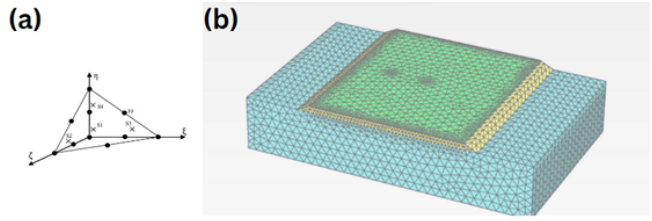


**Figure 3:** Meshing (a)ten noded tetrahedral geometry, (b)connectivity plot of geometry

### 3.3 Analysis

Initial phase: Activation of subgrade, Stress generation within the soil volume is initiated utilizing the K0 procedure.

Phase 1: Activation of the subgrade and pavement layers is performed via the phase explorer window. Geogrid is activated in case of reinforced model.

Phase 2: Activation of the loading condition is conducted to simulate the pavement section's deformation.

## 4. Validations

The IITPave software, developed by IIT Kharagpur, serves as an elastic multilayer linear analysis tool primarily utilized for designing unreinforced pavements via its FPAVE subroutine. In accordance with [3] guidelines, stresses, strains, and deflections under a standard axle load were computed using this software at critical points for unreinforced pavement. This simulation entails structural analysis of unreinforced pavement using IITPave software, necessitating inputs such as layer thicknesses, moduli, Poisson's ratio values, one wheel load of 40 kN, and a tire pressure of 0.56 MPa. Resilient subgrade modulus estimation for various pavement layers is determined based on empirical relationships outlined in Table 1.

The Excel sheet, created by the Department of Roads, is designed to facilitate data input of thickness of different layers, design traffic load, and subgrade CBR. The wheel load, Poisson's ratio, and tire pressure are taken as specified according [2]. Additionally, the resilient modulus of the layers is determined using empirical relationships provided in respective guidelines. The sheet then proceeds to compute vertical strain at the top of the subgrade and horizontal strain at the bottom of the asphalt course. The data from Plaxis 3D, IITPave, and DoR sheet are shown in Table 5 which has shown that the numerical results from Plaxis demonstrate an average variation of 16.2% when compared to the results obtained from IITPAVE software, and an average variation of 16.6% when compared to the results from the DoR sheet. The values from Plaxis 3D, IITPave, and the DoR sheet have been thoroughly examined and verified to adhere to the permissible criteria outlined in the reference, ensuring the safety of the pavement.

**Table 5:** Vertical compressive strains at top of the subgrade

| Vertical Strain at Top of Subgrade with 30 MSA Traffic Load | | | | | | |
|---|---|---|---|---|---|---|
| CBR | 5% | 6% | 7% | 8% | 9% | 10% |
| PLAXIS 3D | 3.81E-04 | 3.63E-04 | 3.44E-04 | 3.23E-04 | 3.17E-04 | 3.15E-04 |
| DoR Sheet | 4.04E-04 | 4.08E-04 | 4.03E-04 | 3.76E-04 | 3.84E-04 | 3.98E-04 |
| IITPave | 3.35E-04 | 3.73E-04 | 3.93E-04 | 3.79E-04 | 4.13E-04 | 4.56E-04 |

## 5. Results and Discussions

The results are obtained by running multiple simulations of a pavement model in Plaxis 3D, as detailed in Table 6. These results encompass findings regarding the optimum placement of geogrid, the enhanced service life of the pavement attributed to geogrid reinforcement, the maximum reduction in pavement thickness post-reinforcement, and the development of a new design catalogue for geogrid-reinforced flexible pavement. Furthermore, a comparison with the design catalogue of [2], without geogrid reinforcement, is also provided.

**Table 6:** Number of finalized numerical model run to assess the results

| CBR (%) | 5 MSA | 10 MSA | 20 MSA | 30 MSA |
|---|---|---|---|---|
| 5 | 12 | 11 | 11 | 12 |
| 6 | 12 | 12 | 12 | 12 |
| 7 | 11 | 12 | 11 | 12 |
| 8 | 11 | 11 | 11 | 12 |
| 9 | 11 | 12 | 11 | 10 |
| 10 | 11 | 10 | 9 | 12 |
| 11 | 11 | 11 | 10 | 12 |
| 12 | 11 | 11 | 10 | 12 |
| 15 | 12 | 12 | 10 | 12 |

### 5.1 Optimum Position

For optimum positioning of geogrid, geogrid is placed in varied position within granular course in Plaxis 3D, where the granular course constitutes the combined thickness of the Wet Mix Macadam (WMM) base and Granular Base Subbase (GBS). In trial 1, the geogrid was positioned at 0% of the base thickness (i.e., asphalt and granular interface). Subsequently, trial 2 involved placing the geogrid at 20% of the granular thickness, while trial 3 positioned it at 60%, trial 4 at 80%, and trial 5 at 100%, maintaining all other criteria same. After each trial, the vertical compressive strain generated at the top of the subgrade is recorded. The data plot illustrating this, ranging from CBR values of 5% to 12%, is depicted in Figure 4. The traffic load remains consistent at 10 MSA for each trial.

Under each test condition, the minimum vertical compressive strain at the top of the subgrade consistently occurred with the geogrid at 100% of the base thickness, followed by 80%. The maximum vertical compressive strain was obtained with the geogrid at 40% of the base thickness, except for a CBR of 6%, where it occurred at 60%. This indicates that the optimum position for geogrid reinforcement is at the granular base-subgrade interface, and it remains fixed for further analysis. Multiple studies [9, 13, 19, 20, 21, 22, 23] have also demonstrated that incorporating geogrids at the interface between a pavement base course and subgrade can substantially enhance pavement performance on weak subgrades, as evidenced by both laboratory tests and full-scale field experiments.

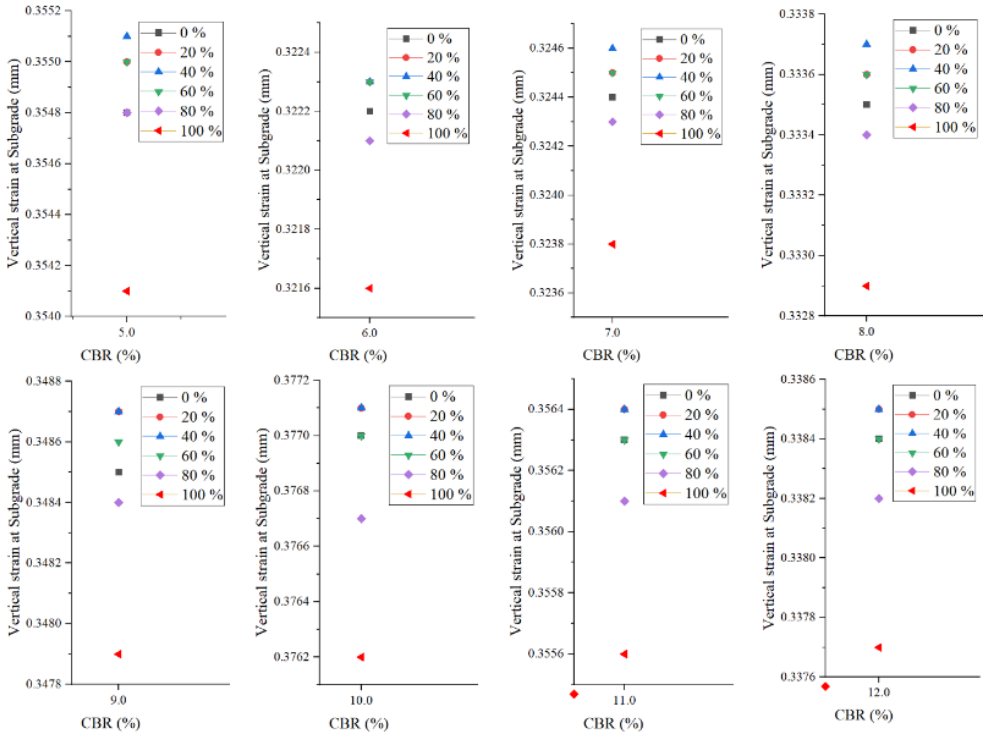


**Figure 4:** Vertical compressive strain produced at the top of the subgrade for varying CBR values from 5% to 12%, under a 10 MSA traffic load, with single layer geogrid reinforcement placed at 0%, 20%, 40%, 60%, 80%, and 100% of the base thickness, measured from the top of the base layer

### 5.2 Geogrid Effectiveness

Once the optimum geogrid position is fixed (at 100% of granular course thickness), Figure 5 compares the vertical compressive strain on subgrade of pavement with single-layer optimum reinforcement against subgrade of unreinforced pavement. It demonstrates a significant reduction in strain with reinforcement, particularly when the subgrade's CBR is lower (23.05% reduction for subgrade of 5% CBR, and 22.95% for subgrade of CBR 6%), decreasing the gap further as the CBR increases. This indicates the possibility of reducing the pavement layer thickness to enhance cost-effectiveness, if not extending its durability.

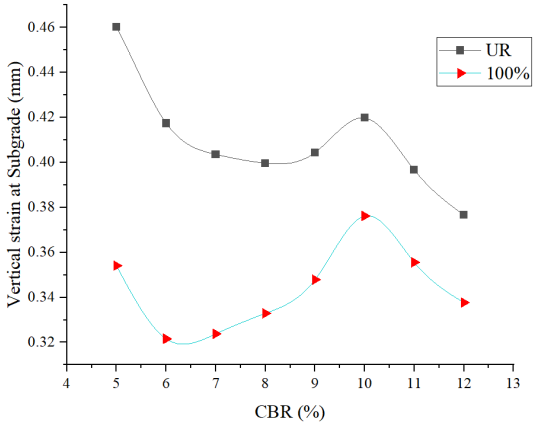


**Figure 5:** Comparison of vertical compressive strain produced at the top of the subgrade of varying CBR values from 5% to 12% when using unreinforced (UR) pavement versus single-layer geogrid reinforcement at 100% of base thickness, with a constant traffic load of 10 MSA throughout

### 5.3 Thickness Reduction

After establishing the optimum geogrid position at 100% of base layer and observing a significant decrease in compressive strain at the top of the subgrade when reinforcement is provided, a subsequent analysis aimed the reduction in the thickness of the combined Wet Mix Macadam (WMM) base and Granular Base Subbase (GBS) of flexible pavement when geogrid reinforcement is provided was conducted using a trial-and-error methodology, with vertical strain at the top of the subgrade as the control parameter. The iterative process consisted of comparing the vertical strain in unreinforced pavement sections with that in reinforced sections, leading to a systematic reduction in the combined granular thickness by approximately 20mm. If the resulting section exhibited lower vertical strain than the unreinforced counterpart, additional reductions in base thickness were implemented until the strain value equal to that of the unreinforced section. While initial thickness reductions were made in 20mm increments, as the difference in strain approached a threshold, the interval was refined to 5 to 10mm for optimum economic considerations. This methodology was systematically applied across all subgrade of CBR values ranging from 5% to 15%, under varying traffic loads of 5 MSA, 10 MSA, 20 MSA and 30 MSA. The outcome of this process yielded novel pavement sections with reduction mentioned in Figure 6, reflecting the impact of geogrid reinforcement on conventional pavement structures.

The results obtained from numerical analysis Figure 6 reveal a consistent trend: as the traffic load increases from 5 MSA to 30 MSA for a CBR value of subgrade, there is increasing reduction in the thickness of the combined base and subbase. This pattern suggests that the geogrid becomes increasingly

efficient with higher traffic loading. This phenomenon is observed across all CBR values. Similarly, for the same traffic load, there is a decrease in base thickness concurrent with an increase in the CBR of the subgrade. This trend is prevalent across most of the CBR values but not at all, indicating that the geogrid performs more effectively in weak subgrade conditions compared to strong subgrade conditions. These findings underscore the significant potential to optimize the thickness of the base, especially in scenarios characterized by high traffic loading and low subgrade CBR.

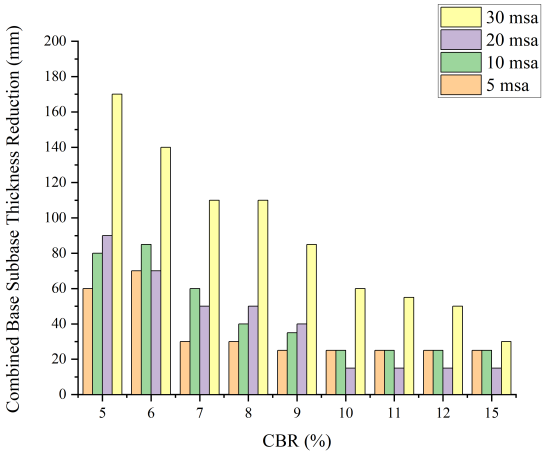


**Figure 6:** Maximum possible reduction in thickness of combined base and subbase of flexible pavement for the subgrade of varying CBR values from 5% to 15% under traffic load of 5 MSA, 10 MSA, 20 MSA and 30 MSA when single layer geogrid is provided at 100% of base thickness

### 5.4 Service Life ratio

The Service Life Ratio (SLR) serves as a metric for evaluating the extension of the service life or durability of a pavement while maintaining a consistent thickness before and after reinforcement. When the thickness remains the same before and after reinforcement, an analysis of the results, as presented in Figure 7, provides insights into the performance. Mathematically, SLR is expressed as the ratio of the vertical compressive strain at the top of the subgrade in the unreinforced state to that observed after reinforcement. This ratio offer a quantitative measure of the improvement in durability achieved through reinforcement while preserving the original pavement thickness. Figure 7 shows substantial enhancement in the service life of the pavement following geogrid reinforcement. Keeping traffic loading constant while allowing for variations in CBR reveals a noteworthy trend: the SLR diminishes with an increase in CBR except for 20 MSA for which slightly irregular trend is observed. This observation suggests that the geogrids increases service life of pavements with weak subgrades more than that with strong subgrade. Conversely, when maintaining a constant CBR and altering the traffic load, the SLR demonstrates an upward trajectory with increasing traffic load where 20 MSA shows slightly different trend. This pattern underscores the efficacy of geogrid reinforcement in handling higher traffic loads from a durability perspective. Importantly, these trends align with the performance of geogrid in thickness reduction scenarios, highlighting a consistent pattern of effectiveness in various conditions.

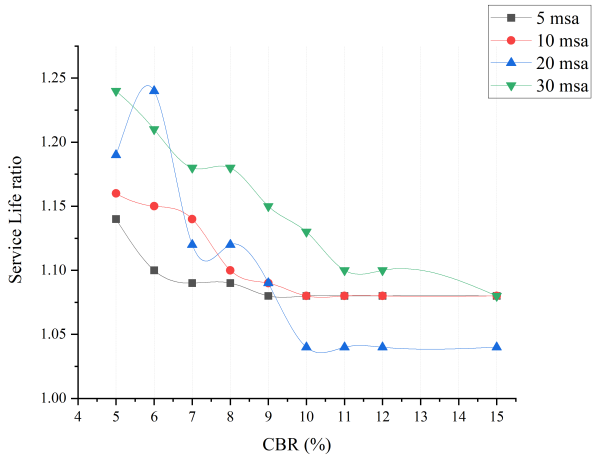


**Figure 7:** Service Life Ratio of flexible pavement for the subgrade of varying CBR values from 5% to 12% under traffic load of 5 MSA, 10 MSA, 20 MSA and 30 MSA when single layer geogrid is provided at 100% of base thickness compared with unreinforced pavement

### 5.5 Design Catalogue

After multiple trial run in Plaxis 3D with geogrid reinforcement at 100% of base thickness and its comparison with unreinforced flexible pavement section as proposed by [2], a set of design catalogue is derived and shown in Figure 8. All the material of pavement layer is same as that proposed by [2]. Only the difference is biaxial geogrid is inserted in subbase and subgrade interface. The proposed design catalogue is for subgrade of CBR range from 5% to 15% and traffic load of 5 MSA, 10 MSA, 20 MSA and 30 MSA for each CBR. The significant decrease in thickness can be economical alternative for conventional flexible pavement with reinforcement in coming days.

## 6. Conclusions

Based on study performed following conclusions are derived:

1. The optimum placement for geogrid reinforcement lies at the interface between the subbase and subgrade layers.

2. When the traffic load remains constant, geogrid performs optimum under lower CBR conditions. Conversely, when the CBR remains consistent, geogrid demonstrates its superior performance under higher traffic loads. In essence, the most effective application of geogrid occurs when there is a combination of lower CBR and higher traffic loads.

3. The reduction in vertical compressive strain shows variability, with the maximum reduction reaching 19.52% under a traffic load of 30 MSA for 5% CBR, while the minimum reduction is observed at 3.62% under a traffic load of 20 MSA for 15% CBR.

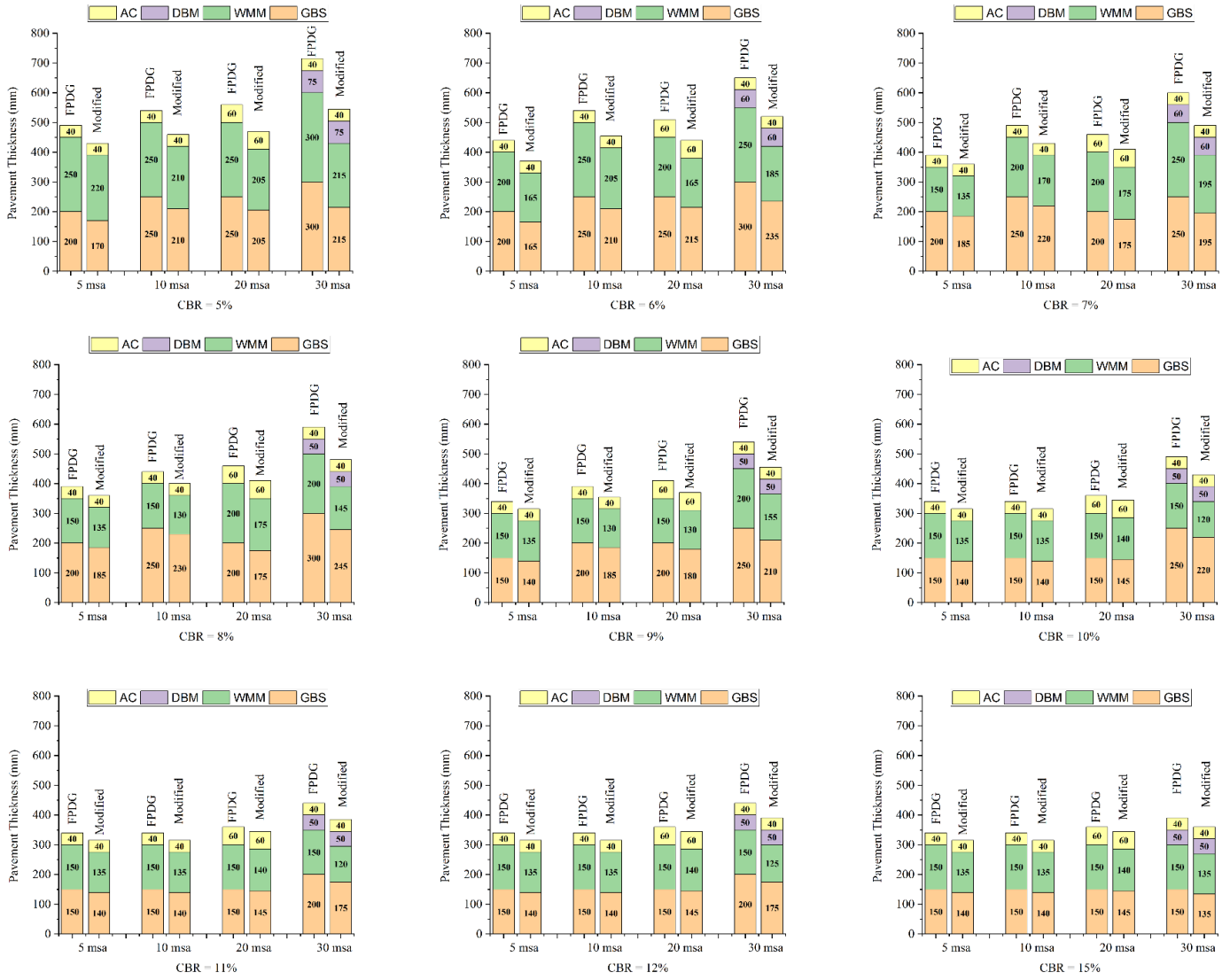


**Figure 8:** Design Catalogue reinforced pavement (Modified) for CBR 5% to 15% and traffic load 5 MSA to 30 MSA and its comparison with [2]

4. The maximum reduction in granular layer thickness varies, starting from 170 mm at 5% CBR and 30 MSA and decreasing to 30 mm at the lowest point, observed for 15% CBR and 30 MSA.

5. The maximum service life ratio ranges from 1.24 at 5% CBR and 30 MSA to 1.08 at 15% CBR and 30 MSA, with values decreasing from the highest to the lowest.

## Author Contributions

Kabin Lamichhane, Dhanapati Dhakal, and Bijay Bhattarai made equal contributions to the conceptualization, methodology, software, analysis, validation, original draft preparation, writing-review and editing of the manuscript. All authors have read and approved the final version for publication.

## Acknowledgements

The authors extend their sincere gratitude to Dr. Ram Chandra Tiwari for his invaluable support and contributions in providing the necessary platform for preparing and analyzing numerical model results. Special thanks are also due to Diwas KC and Bijay Bhusal for their assistance in preparing the numerical model, and to Er. Lok Raj Pant for providing the necessary software.

## References

[1] NS Correia and JG Zornberg. Mechanical response of flexible pavements enhanced with geogrid-reinforced asphalt overlays. *Geosynthetics International*, 23(3):183–193, 2016.

[2] M. Of and P. Planning, Department of Roads. *Flexible Pavement Design Guideline*, second edition, 2021.

[3] Indian Road Congress. *IRC:37-2018 Guidelines for the Design of Flexible Pavements*, 2018.

[4] Murad Abu-Farsakh, Shadi Hanandeh, Louay Mohammad, and Qiming Chen. Performance of geosynthetic reinforced/stabilized paved roads built over soft soil under cyclic plate loads. *Geotextiles and Geomembranes*, 44(6):845–853, 2016.

[5] SK Ahirwar and JN Mandal. Finite element analysis of flexible pavement with geogrids. *Procedia engineering*, 189:411–416, 2017.

[6] Jayhyun Kwon, Erol Tutumluer, and H Konietzky. Aggregate base residual stresses affecting geogrid reinforced flexible pavement response. *International Journal of Pavement Engineering*, 9(4):275–285, 2008.

[7] Hao Wu, Baoshan Huang, Xiang Shu, and Sheng Zhao. Evaluation of geogrid reinforcement effects on unbound granular pavement base courses using loaded wheel tester. *Geotextiles and Geomembranes*, 43(5):462–469, 2015.

[8] Indian Road Congress. *IRC:SP-59 Guidelines for use of geosynthetics in road pavements and associated works*, 2019.

[9] Xiaochao Tang, Shelley M Stoffels, and Angelica M Palomino. Mechanistic-empirical approach to characterizing permanent deformation of reinforced soft soil subgrade. *Geotextiles and Geomembranes*, 44(3):429–441, 2016.

[10] Anil Bhandari and Jie Han. Investigation of geotextile–soil interaction under a cyclic vertical load using the discrete element method. *Geotextiles and geomembranes*, 28(1):33–43, 2010.

[11] Zhijie Wang, Felix Jacobs, and Martin Ziegler. Visualization of load transfer behaviour between geogrid and sand using pfc2d. *Geotextiles and Geomembranes*, 42(2):83–90, 2014.

[12] Steven W Perkins and M Ismeik. A synthesis and evaluation of geosynthetic-reinforced base layers in flexible pavements-part i. *Geosynthetics International*, 4(6):549–604, 1997.

[13] Steve Perkins et al. Evaluation of geosynthetic reinforced flexible pavement systems using two pavement test facilities. Technical report, United States. Federal Highway Administration, 2002.

[14] Ali Khodaii, Shahab Fallah, and Fereidoon Moghadas Nejad. Effects of geosynthetics on reduction of reflection cracking in asphalt overlays. *Geotextiles and Geomembranes*, 27(1):1–8, 2009.

[15] Irene Gonzalez-Torre, Miguel A Calzada-Perez, Angel Vega-Zamanillo, and Daniel Castro-Fresno. Experimental study of the behaviour of different geosynthetics as anti-reflective cracking systems using a combined-load fatigue test. *Geotextiles and Geomembranes*, 43(4):345–350, 2015.

[16] JN Prieto, J Gallego, and I Perez. Application of the wheel reflective cracking test for assessing geosynthetics in anti-reflection pavement cracking systems. *Geosynthetics International*, 14(5):287–297, 2007.

[17] Connect edition v21.00 plaxis 3d-reference manual.

[18] RL Terrel, IS Awad, and LR Foss. Techniques for characterizing bituminous materials using a versatile triaxial testing system. In *Fatigue and Dynamic Testing of Bituminous Mixtures*. ASTM International, 1974.

[19] Abbas F Jasim, Mohammed Y Fattah, Israa F Al-Saadi, and Alaa S Abbas. Geogrid reinforcement optimal location under different tire contact stress assumptions. *International Journal of Pavement Research and Technology*, 14:357–365, 2021.

[20] Imad L Al-Qadi, Thomas L Brandon, Richard J Valentine, Bruce A Lacina, and Timothy E Smith. Laboratory evaluation of geosynthetic-reinforced pavement sections. *Transportation research record*, (1439):25–31, 1994.

[21] Imad L Al-Qadi, Erol Tutumluer, Jayhyun Kwon, and Samer H Dessouky. Accelerated full-scale testing of geogrid-reinforced flexible pavements. Technical report, 2007.

[22] Steven W Perkins et al. Geosynthetic reinforcement of flexible pavements: laboratory based pavement test sections. Technical report, Montana. Department of Transportation, 1999.

[23] Rudolf Hufenus, Rudolf Rueegger, Robert Banjac, Pierre Mayor, Sarah M Springman, and Rolf Brönnimann. Full-scale field tests on geosynthetic reinforced unpaved roads on soft subgrade. *Geotextiles and Geomembranes*, 24(1):21–37, 2006.